Astron. Astrophys. 334, 325–336 (1998)

ASTRONOMY AND ASTROPHYSICS

The Hipparcos solar system objects catalogues⋆

D.Hestroffer[1,2], B. Morando[2⋆⋆], E. Høg[3], J. Kovalevsky[4], L. Lindegren[5], and F. Mignard[4]

[1] Astrophysics Division, Space Science Department of ESA, ESTEC, Postbus 299, 2200 AG Noordwijk, The Netherlands
[2] Bureau Des Longitudes, URA CNRS 707, 77 Avenue Denfert Rochereau, F-75014 Paris, France
[3] Copenhagen University Observatory, Juliane Maries Vej 30, DK-2100 Copenhagen O., Denmark
[4] Observatoire de la Côte d'Azur, Département CERGA, UMR CNRS 6527, Av. N. Copernic, F-06130 Grasse, France
[5] Lund Observatory, Box 43, S-22100 Lund, Sweden

Received 15 October 1997 / Accepted 28 January 1998

Abstract. Astrometric and photometric measurements of a number of solar system objects were performed by the Hipparcos satellite in both the Hipparcos main mission and the Tycho experiment. The results concern mainly asteroids but also the planetary satellites Europa, Ganymede, Callisto, Titan and Iapetus, and the major planets Uranus and Neptune. The specific aspects of the Tycho/Hipparcos observations and reduction process implemented for the solar system objects are presented. Special attention is paid to the error budget of the reduction which is accurate to the mas (milliarcsecond) level for the Hipparcos main mission. The contents of the Hipparcos and Tycho Solar System Objects Catalogues are briefly described. Comparison between the results derived from the two Consortia FAST and NDAC, as well as comparisons with ground-based observations, are given.

Key words: astrometry – solar system: general – methods: data analysis – catalogs

1. Introduction

Along with the thousands of stars observed by the satellite, the observing programme included a selection of solar system objects (major planets, planetary satellites and asteroids). The primary motivation underlying their observation was to provide highly accurate positions for the link of the dynamical reference system to the International Celestial Reference System (ICRS), but also to enable dynamical and physical studies of these objects. The value of astrometric observations of asteroids – relative to the reference frame defined by the stars – for the establishment of the dynamical reference frame, was first suggested by Dyson (1928). These objects were thought to considerably enhance the results obtained from observations of the Sun or major planets. Nonetheless, the theoretical precision estimated by Clemence (1948) has never been reached; hence such observations of minor planets enter for instance in the solution derived by Fricke (1982) for the FK5 with a relatively modest weight. Hipparcos should dramatically improve the situation (e.g. Hestroffer et al. 1995; Bec-Borsenberger et al. 1995), and yield a link between the dynamical system and the ICRS with a precision of the same order of magnitude as the best result obtained so far by other means (Folkner et al. 1994).

High precision measurements of the positions of asteroids enable improvement of their ephemerides but also, in particular cases of very close encounter, to determine the mass of some of them (e.g. Scholl et al. 1987; Viateau & Rapaport 1997; Hilton 1997). Also the observations of planetary satellites relative to the background stars yield, in an indirect manner, accurate positions of the gravitating major planet's centre of mass (e.g. Morrison et al. 1997; Fienga et al. 1997). Photometric observations of asteroids provide information about their rotational properties such as shape and spin-vector orientation (Harris & Lupishko 1989), and the scattering properties of their surface (Bowell et al. 1989). Hence observations of such objects yield insight into their collisional evolution, and into the early solar system.

The Hipparcos satellite successfully observed the solar system objects contained in the pre-defined programme during its ~ 3.3-year mission duration. Hence it provides astrometric as well as photometric information on these relatively bright objects. The information gathered by the star mapper constitutes the Tycho Catalogue, while the Hipparcos Catalogue is derived from the observations made through the main grid. The reduction of the observations of the solar system objects although being a special task, followed in the first stages the procedure applied to the programme stars. In particular the intermediate astrometric positions on the sky and the photometry are provided as an output of a general reduction process that encompassed all observed objects. In this sense, this paper presents the specific reduction schemes applied to the rapidly moving and eventually resolved solar system objects, but not an exhaustive description of the whole reduction process.

Send offprint requests to: D. Hestroffer/Present address: OATO, Str. Osservatorio 20, I-10025 Pino Torinese (TO), Italy (hestro@fortuna.to.astro.it)

⋆ Based on data from the Hipparcos astrometry satellite

⋆⋆ Deceased. Co-leader of the solar system observations for the Hipparcos Data Analysis

The selected objects, the ground-based campaign of observations pre-launch, and the Hipparcos geometry of observations are briefly presented in Sect. 2. The Tycho and Hipparcos data are of different nature and precision, and are presented separately in Sect. 3 and Sect. 4. All astrometric positions are given in the ICRS, the transformation to which is presented in Sect. 5. The precision of the measurements, and comparison with ground based observations or calculated places, and between the NDAC and FAST positions, are given in Sect. 6.

2. The Hipparcos satellite observations

2.1. Observing programme

Initially two satellites (Europa and Titan) and 63 asteroids were included in the Hipparcos (main mission) observing programme. Positions of the solar system objects entered in the Hipparcos Input Catalogue by means of their ephemerides (Bec-Borsenberger 1985). Since the positions had to be known a priori with a precision better than 1 arcsec, a ground-based observation campaign of these asteroids was started in 1983 in order to improve the accuracy of their ephemerides. Observations were carried out with the meridian circles of Bordeaux and La Palma, and the astrographs of the Marina observatory (San Fernando) and the Fabra observatory (Barcelona). The number of selected asteroids was reduced to 48 after consideration of the number of predicted transits during the scheduled nominal mission duration (Bec-Borsenberger 1989). The Saturnian satellite S VIII Iapetus was added to the observation programme during the mission. A priori ephemerides of the 48 Hipparcos asteroids, the four Galilean satellites, Titan, Venus and planets Mars through Neptune were also calculated as part of the Tycho Input Catalogue of 3 million stars. Nevertheless, not all of these solar system objects were retained for the final Catalogue (see Sect. 3), but their inclusion was necessary for technical reasons (Bastian & Wagner 1997).

2.2. A scanning satellite

Since the Hipparcos satellite scanned the whole sky in a regular manner enabling a complete and reasonably uniform coverage of the celestial sphere, no pointing to a specific object was possible; but an observation occurred during its transit across the field of view. Moreover, in order to prevent scattered light from the Sun and strong thermal fluctuation during the satellite rotation, the spin axis of the satellite precessed with a period of 57 days and a constant angle of 43° around the direction towards the Sun. Since solar system objects are gravitating around the Sun in a band near the ecliptic, observations of these objects were spread around the quadratures (see Fig. 1), i.e. when the solar phase angle was maximal. As shown in Fig. 2, the phase angle of a Hipparcos asteroid was always larger than 10° with a typical value of 20°. Consequently, the solar phase angle can in general not be neglected, neither for the photometric nor for the astrometric data. The two fields of view of the telescope (separated by a 58° angle) scanned a great circle perpendicular to the spin axis. Over a time scale of one day, observations

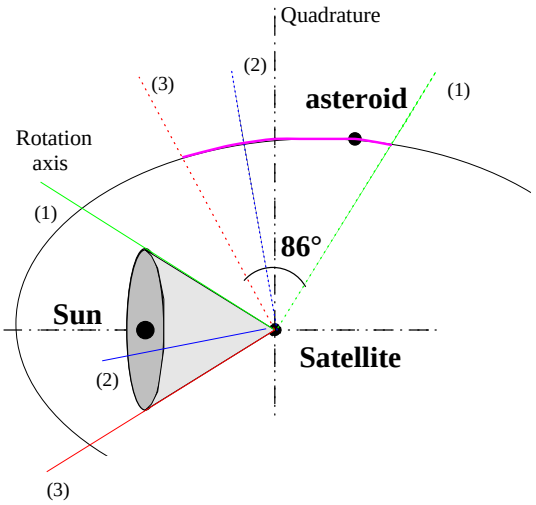

Fig. 1. Schematic view of the Hipparcos satellite scanning procedure (or scanning law). The rotation axis describes a cone around the direction of the Sun. The observations of solar system objects, at right angle to the rotation axis, were made around the quadratures, bounded by positions (1) and (3)

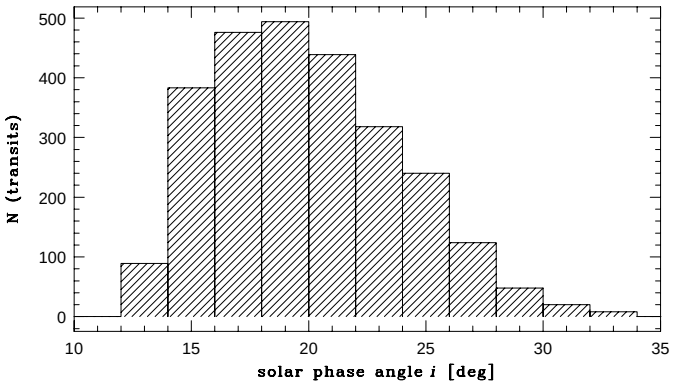

Fig. 2. Distribution of the solar phase angle of the minor planets during the Hipparcos mission. The scanning law implied that the observations could only occur in the vicinity of the quadratures, in contrast with the prevailing situation for ground-based observations which are normally concentrated around opposition.

were separated over successive scans by the 20.6 min between a preceding and following field of view transit, followed by an interval of 107.4 min before the object again may have crossed the preceding field of view. The number of observations varied between the different objects (from roughly 15 to 125 transits). The same remark applies to the distribution of these transits in time or along the planet's trajectory. The Hipparcos and Tycho observations were almost simultaneous; a transit across the star mapper occurred a few seconds before the transit across the main grid.

2.3. Ephemeris and photometric systems

The ephemerides used for the satellite observations were compressed with an internal accuracy of 0.5 arcsec in the form of Chebyschev polynomials. For the reductions, the computed

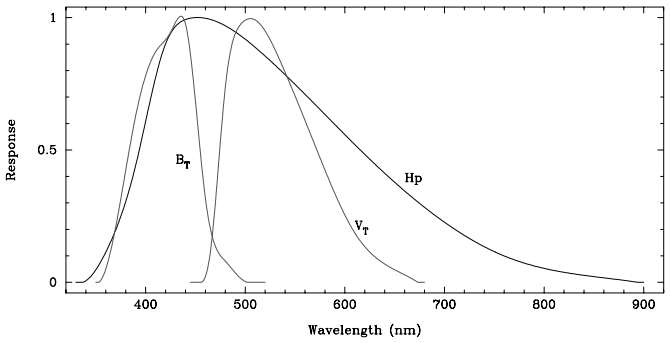

Fig. 3. Hipparcos (Hp) and Tycho (B_T, V_T) photometric systems.

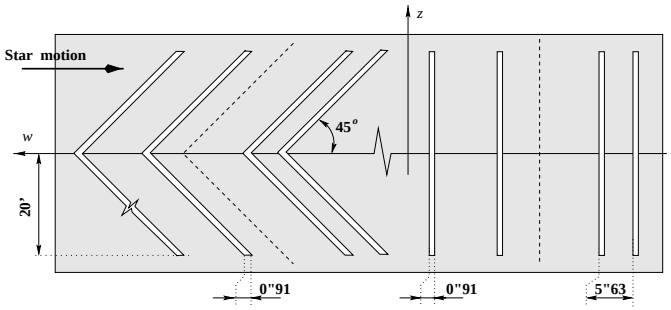

Fig. 4. Schematic view of the star mapper slits system. All slits have the same width in the direction of the w axis. The inclined and vertical slits are spaced, in the direction of a star's motion, at distance ratios 2:3:1 of the step $s = 5.63$ arcsec. The 'fiducial lines', which can be thought as the centres of gravity of the four slits in each group, are shown as dashed lines

positions of each minor planet at each observation epoch were determined by numerical integration from osculating elements taken from the "Ephemerides of minor planets for the year 1992" (Batrakov 1991). Only the perturbations by the major planets were taken into account. Ephemerides of the Galilean satellites were determined by use of the the G-5 theory (Arlot 1982), while the theory of Dourneau (1993) was used for the Saturnian satellites. The positions of the major planets were calculated from the DE200 ephemeris (Standish 1990). The velocity for the Earth, as part of the whole Hipparcos reduction procedure, made use of the VSOP 82/ELP 2000 theory (Bretagnon 1982; Chapront-Touzé & Chapront 1983). The geocentric Hipparcos satellite ephemeris was provided by the operation centre (ESOC) with an accuracy of ∼1.5 km in position and ∼ 0.2 m/s in velocity.

The Hipparcos and Tycho photometric systems are related to the particular detectors and filters used and are not standard systems (van Leeuwen et al. 1997). The Hipparcos main instrument observed in a broad-band system (Hp) in order to optimize the astrometric signal. The Tycho observations were carried out in two filters (B_T, V_T) which are somewhat similar to the Johnson B and V bands. Fig. 3 shows the various passbands. Details are given in Sect. 1.3 of Volume 1 of the Hipparcos and Tycho Catalogues (ESA 1997), in Mignard et al. (1997) and in Großmann (1997). Over the range $-0.2 < (B-V)_T < 1.8$, the following linear formulae yield transformations between the Tycho and Johnson scales accurate to 0.05 mag:

$$\begin{aligned} V_T - V_J &= 0.09\,(B-V)_T \\ (B-V)_J &= 0.85\,(B-V)_T \end{aligned}$$

The transformation from the Hp system to standard magnitudes is given by Mignard et al. (1997). The Hp and V_J bands have more or less the same effective wavelength, and they can be related with a good approximation for solar system objects (with $-0.5 \lesssim B-V \lesssim 1.5$) by:

$$\begin{aligned} Hp - V_J \sim\ & 0.304\,(B-V) - 0.202\,(B-V)^2 \\ & +0.107\,(B-V)^3 - 0.045\,(B-V)^4 \end{aligned}$$

The zero points of the magnitude scales are defined such that $Hp = V_T = V_J$ and $B_T = B_J$ at $B-V = 0$.

Table 1. Solar system objects of the Tycho Catalogue

Name	Photometry	Astrometry
Minor planets:		
(1) Ceres	√	√
(2) Pallas	√	√
(4) Vesta	√	√
(6) Hebe	√	√
(7) Iris	√	√
Satellites:		
J III–Ganymede	–	√
J IV–Callisto	–	√
S VI–Titan	√	√
Major planets:		
Uranus	–	√
Neptune	–	√

3. Tycho

3.1. Star mapper

A schematic view of the grid system is given in Fig. 4. The Tycho observations were not adapted to objects larger in apparent size than the smallest separation between two slits (5.63 arcsec). For this reason no Tycho data are provided for Venus, Mars, Jupiter and Saturn. Objects brighter than $V \sim 10$ and with sufficient number of observations were retained; the list is given in Table 1. When available, the photometry is provided in the Tycho B_T and V_T passbands.

The magnitudes in the two channels were derived, in the same way as for the stars, from the amplitude of the convolved signal and were calculated by a simplified calibration procedure. The magnitude provided for each transit corresponds to the mean for each slit group crossing. The primary astrometric and photometric information is obtained from the convolved signal, where the magnitude is derived from its amplitude (Fig. 5). Hence no magnitude is provided for objects larger in apparent size than the width of the slits (0.91 arcsec). For objects that were not substantially smaller than the slit width, systematic er-

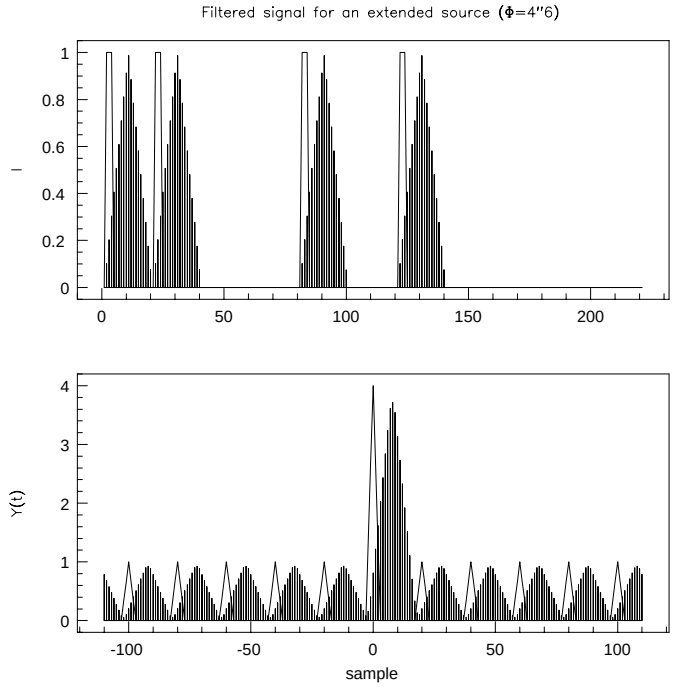

Fig. 5. Simplified profile for the photon count of a point-like source and a circular extended object of apparent diameter $\phi = 4.6$ arcsec (top). Both intensities are normalised to unity. This signal is folded by a digitalised filter (bottom); the position and amplitude are then derived from the Q integer detection filter [-1,-1,-1,0,+1,+1,+1]

rors may occur. Finally, no standard errors are provided for the estimation of the B_T and V_T magnitudes; they are of the order of 0.1 mag for an object of magnitude $V \sim 8$ and 0.35 mag for $V \sim 10$.

3.2. Astrometry

Since the transits across each slit group yield information in two directions, a conventional $(\alpha,\, \delta)$ two-dimensional position on the celestial sphere could be derived for each transit. The displacement of the rapidly moving solar system object between the crossing of the fiducial lines of the slit groups (in a time interval up to about 10 s) is known with sufficient accuracy to enable such a construction. The primary astrometric information is the time when an object crossed the fiducial line as derived in the detection and estimation process. The difference between the observed and predicted crossing time for each slit group was converted into an along-scan residual in position. Next, the two along-scan residuals $(\Delta u_1,\, \Delta u_2)$ were transformed into residuals in the two orthogonal directions w and z in the focal plane of the telescope. This transformation $\boldsymbol{P}$ depends on the sign of the z coordinate, whether the transit occurred in the upper part (sgn$(z) = +1$) or the lower part (sgn$(z) = -1$) of the inclined slits. The orientation of the $(\mathbf{w},\, \mathbf{z})$ frame on the celestial sphere is given by the position angle θ, the angle in the tangent plane between $\mathbf{w}$ and north counted positive from north through east. The observed position, at the — arbitrarily chosen — reference epoch t_2, is thus derived from an a priori calculated position (close to the true position) and the along-scan residuals by:

$$\begin{pmatrix} \Delta\alpha_2 * \\ \Delta\delta_2 \end{pmatrix} = \boldsymbol{Q}\ \boldsymbol{P} \begin{pmatrix} \Delta u_1 \\ \Delta u_2 \end{pmatrix} \tag{1}$$

where $\Delta\alpha_2 * = \Delta\alpha_2 \cos\delta_2$, and:

$$\boldsymbol{Q} = \begin{pmatrix} \sin\theta & -\cos\theta \\ \cos\theta & \sin\theta \end{pmatrix}; \boldsymbol{P} = \begin{pmatrix} 0 & 1 \\ \mathrm{sign}(z) & -\mathrm{sign}(z) \end{pmatrix} \tag{2}$$

The second-order terms arising from the transformation between the tangent plane and the celestial sphere are neglected. Introducing the diagonal matrix of the standard error of the measurements:

$$\boldsymbol{\sigma} = \begin{pmatrix} \sigma_1 & 0 \\ 0 & \sigma_2 \end{pmatrix}$$

the variance matrix of the derived coordinates is given by:

$$\begin{pmatrix} \sigma^2_{\alpha *} & \sigma_{\alpha *}\,\sigma_\delta\,\rho^\delta_{\alpha *} \\ \sigma_{\alpha *}\,\sigma_\delta\,\rho^\delta_{\alpha *} & \sigma^2_\delta \end{pmatrix} = \boldsymbol{Q}\ \boldsymbol{P}\ \boldsymbol{\sigma^2}\ \boldsymbol{P'}\ \boldsymbol{Q'} \tag{3}$$

This matrix is no longer diagonal, reflecting the fact that - depending on the position angle θ and the ratio σ_2/σ_1 - the principal axes of the associated error ellipse do not coincide with the (N,E) directions toward the northern celestial pole and the east. In the coordinate system $(\mathbf{w};\, \mathbf{z})$ defined by the star mapper geometry, the orientation and size of the error ellipsoid is given by the quadratic form associated with $\boldsymbol{P}\ \boldsymbol{\sigma^2}\ \boldsymbol{P'}$. Putting $k = \sigma_2^2/\sigma_1^2$, the diagonalisation of the previous matrix yields the principal axes of the error ellipse (see Fig. 6):

$$\begin{aligned} \lambda_1 &= \frac{\left(1 + 2\,k - \sqrt{1 + 4\,k^2}\right)}{2}\ \sigma_1^2\ e_1 \\ \lambda_2 &= \frac{\left(1 + 2\,k + \sqrt{1 + 4\,k^2}\right)}{2}\ \sigma_1^2\ e_2 \end{aligned} \tag{4}$$

where λ_1 and and λ_2 are the semi-minor and semi-major axes respectively. The directions are given by the non-unit vectors $\mathbf{e}_1$ and $\mathbf{e}_2$ whose components are:

$$\begin{aligned} \mathbf{e}_1 &= \left(1 + \mathrm{sign}(z)\,\sqrt{1 + 4\,k^2},\ 2\,k\right) \\ \mathbf{e}_2 &= \left(1 - \mathrm{sign}(z)\,\sqrt{1 + 4\,k^2},\ 2\,k\right) \end{aligned} \tag{5}$$

The along-scan standard errors are derived from an error model suitable for stellar images and do not correspond to Gaussian noise. Moreover, as shown in Fig. 5, the signals for planets are broader and flatter at the top than the signals of point-like sources. Thus the derived quantities $\sigma^2_{\alpha *}$ and σ^2_δ should more preferably be regarded as indicators of the quality of a single measure.

For each transit, the astrometric observation is defined by the reference epoch t_2, the coordinates $(\alpha,\, \delta)$, the standard errors $\sigma_{\alpha *},\, \sigma_\delta$ and the correlation between the two coordinates $\rho^\delta_{\alpha *}$. To enable future systematic correction of the data, especially for the large major planets, the position angle θ, the inclined-slit

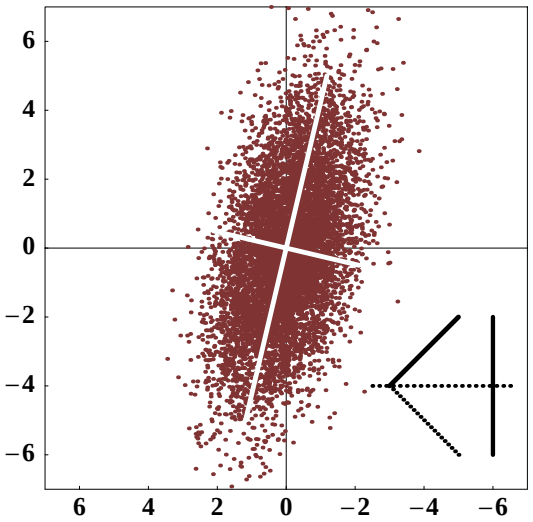

Fig. 6. Confidence ellipse associated with the Tycho astrometry of solar system objects in the $(\mathbf{w};\,\mathbf{z})$ coordinate system. Numerical simulation obtained by assuming that the quantities $(\Delta u_1,\,\Delta u_2)$ follow a normal distribution, and scaled in units of σ_2. The graph is given for a transit in the upper part of the inclined slits, with realistic variance ratio ($k = 1/4$)

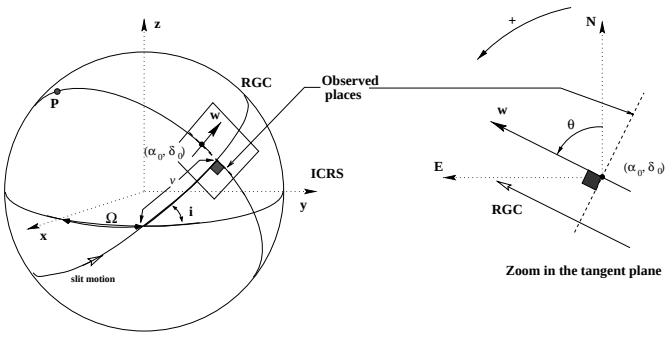

Fig. 7. One dimensional position locus for the Hipparcos main-mission observations of solar system objects. Reference point on the celestial sphere (left) and transformation to the tangent plane (right)

flag sign(z), and the standard errors $\sigma_1,\,\sigma_2$ are provided as additional data. All positions are referred to the ICRS system (see Sect. 5). It is stressed that phase, shape or albedo corrections are not taken into account. The given position corresponds to the photocentre for the smallest objects. For Uranus, Neptune and to a lesser extent the two Jovian satellites, whose angular diameters are larger than the slit width, the position on the surface of the body depends highly on its albedo distribution and the scanning geometry. More accurate correction to the centre of figure can be applied by a simulation of the Tycho photon counts and convolution with the slit response. A general description of the appropriate procedure is given by Høg et al. (1997).

Table 2. List of minor planets observed by Hipparcos (main mission)

(1) Ceres	(18) Melpomene	(63) Ausonia
(2) Pallas	(19) Fortuna	(88) Thisbe
(3) Juno	(20) Massalia	(115) Thyra
(4) Vesta	(22) Kalliope	(129) Antigone
(5) Astraea	(23) Thalia	(192) Nausikaa
(6) Hebe	(27) Euterpe	(196) Philomela
(7) Iris	(28) Bellona	(216) Kleopatra
(8) Flora	(29) Amphitrite	(230) Athamantis
(9) Metis	(30) Urania	(324) Bamberga
(10) Hygiea	(31) Euphrosyne	(349) Dembowska
(11) Parthenope	(37) Fides	(354) Eleonora
(12) Victoria	(39) Laetitia	(451) Patientia
(13) Egeria	(40) Harmonia	(471) Papagena
(14) Irene	(42) Isis	(511) Davida
(15) Eunomia	(44) Nysa	(532) Herculina
(16) Psyche	(51) Nemausa	(704) Interamnia

Table 3. Availability and sources of main mission astrometry and photometry for solar system objects

Object	Astrometry	Photometry
Minor planets	FAST+NDAC	FAST
J II Europa	NDAC	(not available)
S VI Titan	NDAC	(not available)
S VIII Iapetus	FAST+NDAC	(not available)

4. Hipparcos (main mission)

4.1. Main grid

In contrast to the star mapper, the main grid consisted of 'vertical' slits only, and hence only provides a one-dimensional position, i.e. the observed position locus in the direction perpendicular to the slits (see Fig. 7). The main grid consists of 2688 narrow transparent slits with an average width of 3.13 μm and a regular average separation of 8.20 μm, yielding the grid step (or grid period) $s = 1.2074$ arcsec when projected on the sky. Observation with this main grid were primarily limited by the object's magnitude and by its size. The continuously scanning satellite yielded a limited duration of photon acquisition, and thus a limiting magnitude of the order of $V \sim 13$. Highly resolved objects were too large to enable an accurate position with the grid, limiting thus the number of observed natural satellites. The list of observed objects is given in Tables 2 and 3.

The primary astrometric and photometric information was obtained from the modulated signal. For a point-like source, the Hipparcos modulated (phase calibrated) signal can be expanded in a Fourier series as:

$$S(t) = I_0\,[1 + M_0\cos(\omega t + \varphi_0) + N_0\cos(2\,\omega t + 2\,\varphi_0)] \quad (6)$$

where M_0, N_0 are calibrated modulation coefficients, φ_0 is the modulation phase of the signal irrespective of the harmonic. It corresponds to the position of the source on the grid from the centre of the nearest slit at the reference time $t = 0$. With a displacement at a velocity V in the direction perpendicular to the slits, $\omega = 2\pi\,V/s$ is the fundamental angular frequency of the signal. For sources of significant size, integration of the

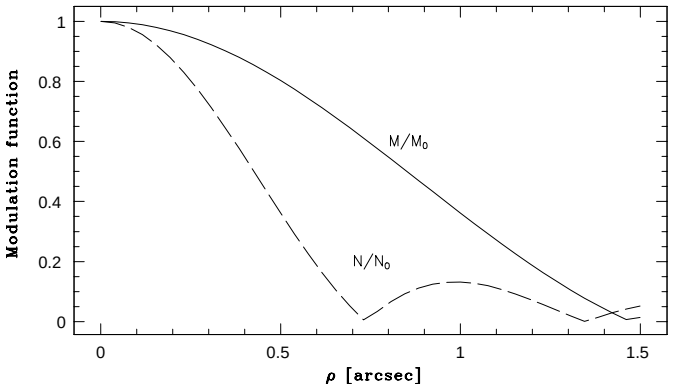

Fig. 8. Modulation function for the first two harmonics of a uniformly bright disc as a function of the apparent diameter ρ

basic relation in Eq. (6) yields a similar Fourier series (Morando 1987, Lindegren 1987, Morando & Lindegren 1989):

$$S(t) = I\,[1 + M\cos(\omega t + \varphi) + N\cos(2\,\omega t + 2\,\psi)] \qquad (7)$$

where the modulation amplitudes M and N are degraded, and the phases φ and ψ are in general different and shifted with respect to the body's geometric barycentre. Introducing the dimensionless spatial frequency $x = \pi\rho/s$, where ρ is the apparent diameter of a spherical object, one find for a uniformly bright disc the degradation of the modulation amplitudes or modulation function (Hestroffer & Mignard 1997a, 1997b):

$$\begin{aligned} M(x)/M_0 &= \left|\,{}_0F_1(2;\,-x^2/4)\,\right| = 2\,\frac{|\,J_1\,(x)\,|}{x} \\ N(x)/N_0 &= M/M_0(2\,x) \end{aligned} \qquad (8)$$

where ${}_0F_1$ and J_1 are the hypergeometric and Bessel functions respectively. A first consequence of this degradation is that objects larger than approximately 1 arcsec yield a signal too flat to enable an accurate determination of the phases and consequently of their positions on the grid (see Fig. 8). Thus only small solar system objects could be added to the main mission observation programme.

The phase shifts for a uniformly bright disc can be computed by means of the complex function:

$$\begin{aligned} U(x) &= J_1(x) + J_1(x\cos i) + \\ &\qquad \sqrt{-1}\,\left[\mathbf{H}_1(x) - \mathbf{H}_1(x\cos i)\right] \end{aligned} \qquad (9)$$

where i is the solar phase angle and $\mathbf{H}_1$ the Struve function. For a scan along the intensity equator the phase offsets relative to the centre of figure is:

$$\begin{aligned} \Delta\varphi &= \arg\,[U(x)] \\ \Delta\psi &= \tfrac{1}{2}\arg\,[U(2x)] \end{aligned} \qquad (10)$$

4.2. Photometry

Photometry is provided from the FAST Consortium's reductions for the 48 asteroids of the mission. No photometry is available for the planetary satellites since the diffusion of the light of their respective planets considerably perturbed the measurements (see Sect. 4.4). The reduction of the data was similar to that adopted for the stars. The apparent magnitudes are provided in the Hipparcos Hp broad-band photometric system for every transit, where an a priori value of the colour index $B - V = 0.5$ mag was used. The observed magnitudes of minor planets being accurate to a few hundredth of a magnitude, the correction to the geocentre was neglected. Over the observation period, the solar system barycentre was always within 1.6 solar radii of the centre of the Sun, so that the offset distance barycentre–centre of the Sun may also be disregarded.

Two estimators of the apparent magnitude ($Hp_{\rm dc}$ and $Hp_{\rm ac}$) were derived from the coefficients I, IM, IN in Eq. (7). The apparent magnitude $Hp_{\rm dc}$ is directly given by the mean intensity I corrected for background noise. The second estimator $Hp_{\rm ac}$ is derived from the amplitude IM, IN of the modulation. The $Hp_{\rm ac}$ estimator, given as additional data, is of lower precision and biased. For a spherical object of apparent diameter ρ, we have:

$$\Delta H = Hp_{\rm ac} - Hp_{\rm dc} \sim a\,\rho^2 + o\,(\rho^4) + o\,(i) \qquad (11)$$

where i is the solar phase angle, and $a > 0$ is a scalar depending on the actual brightness distribution; we find $a = 1.214$ mag/arcsec^2 for a uniformly bright disc. For the smallest asteroids, the difference between these two determinations is however smaller than the measurement noise.

Due to the rather random observation epochs of the objects, the data rarely yield magnitudes over a rotation period, nor representative light curves. They can nevertheless be used for deriving magnitudes reduced to unit heliocentric and geocentric distances (accurate to about 0.03 mag) over a large range of solar phase angles, rotational phase, aspect and obliquity. The Hipparcos solar system objects photometric catalogue is completed, for convenience, with some additional calculated aspect data: the distance to the Sun, the distance to the satellite, and the solar phase angle.

4.3. Astrometry

As for the stars, the astrometry is given at an intermediary stage by an abscissa v over a reference great circle (RGC, see Fig. 7). This abscissa is derived from Eq. (7) by weighted mean of the modulation phases $0.75\,\varphi + 0.25\,\psi$ within FAST, and the phase φ, of the first harmonic only, within NDAC. For a point-like or relatively small source (typically with a diameter $\rho \lesssim 0.05$ arcsec), the FAST and NDAC abscissae have the same value since the calibrated phases φ and ψ are (almost) equal. For a larger extended source, the difference between the FAST and NDAC abscissa depends on the physical properties of the minor planet or planetary satellite (such as the apparent diameter, solar phase angle, albedo distribution over the visible surface and scanning geometry). The position derived from the phases of the modulated signal is also shifted with respect to the photocentre. The difference between the photocentre and the position assigned from the phases, using the FAST and NDAC procedures,

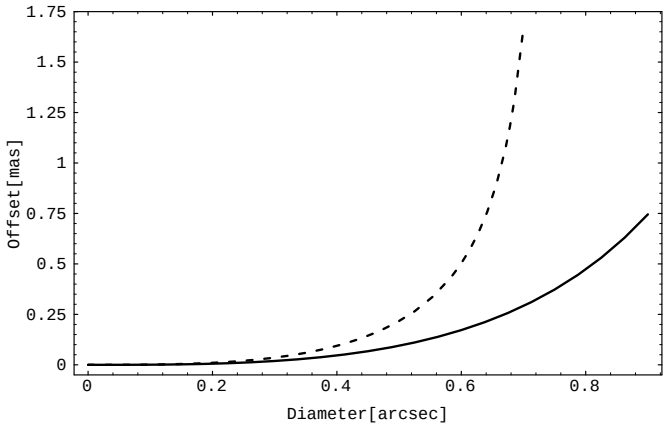

Fig. 9. Theoretical difference between the observed position and the photocentre versus apparent diameter. The graphs correspond to a spherical object of uniform brightness viewed with a solar phase angle $\alpha = 20^\circ$. Solid curve: positions derived from the first harmonic only (NDAC). Dotted curve: positions derived from a weighted mean of the harmonics (FAST) — this method is in practice limited to objects smaller than 0.7 arcsec

is shown in Fig. 9 as a function of the apparent diameter of a uniformly bright planet. For a phase angle of $\alpha = 20^\circ$, typical for the Hipparcos observations of minor planets (see Fig. 2), the differences do not significantly exceed one milliarcsec except for (1) Ceres as observed by FAST at its maximum diameter, $\rho \sim 0.7$ arcsec.

To obtain the one-dimensional position on the grid in the scanning direction, one makes use of the a priori position of the observed object obtained from the calculated ephemeris. The resulting position locus can however be erroneous by a multiple of the grid period. Its validity was verified in comparison with the improved ephemerides obtained after incorporating the Hipparcos observations. As a rule, abscissae differing from the calculated one by more than 0.801 arcsec in modulus were corrected by one grid period. This correction was only necessary for a very small number of observations. Nevertheless no satisfactory solution was found for the observations of minor planet (27) Euterpe; this means that some of the transits may be suspicious, or erroneous by one grid period.

4.4. Planetary satellites

The reduction of the planetary satellites was more problematic because of their relatively large size, and their proximity to the bright major planet. The proximity of a bright object in the instantaneous field of view considerably perturbed the observations, and for the three satellites of the programme no satisfactory photometric solution could be reached. The average instantaneous field of view profile is given for large offsets in Fig. 10. With a planet 7 or 8 magnitudes brighter than the satellite and located only a few hundreds of arcsec from the centre of the field of view, there is still some planetary light perturbing the satellite signal. The effect is hard to assess because the exact attenuation profile was not known in the periphery of the instantaneous field of view. Fig. 10 (right) shows the difference between the two magnitude scales $Hp_{\rm ac}$ and $Hp_{\rm dc}$ after a first approximation of the expected effect due to the apparent size of a satellite, given by Eq. (11), has been removed. The remaining difference, which should be close to zero, has been sampled as a function of the separation between the satellite and the planet at the time of observation. This non-modeled difference reflects essentially the residual disturbing light originating from the planet. The consequences for the photometric measurement are fairly large for any of the planetary satellites J II Europa, S VI Titan and S VIII Iapetus whatever the separation to such an extent that no reliable magnitude could be provided.

The effect of this scattered light on the astrometry is considerably diminished since it provides essentially an unmodulated background noise. Other satellites may also perturb the observations, in particular for Europa because in 1991 the Earth was close to the orbital plane of the Jovian satellites. Such erroneous observations were filtered (see Sect. 4.5). As can be seen in Fig. 8, the FAST astrometric reduction procedure is unsuitable for objects with an apparent diameter larger than approximately 0.7 arcsec, i.e. when the second harmonic amplitude is too small to derive an accurate estimate of the phase ψ. However this does not affect the NDAC reduction scheme, thus only the NDAC astrometry of J II Europa and S VI Titan is published. Scattered light, whose origin was not well understood, perturbed the measurements of the Saturnian satellites occurring over a five day interval ($8972 \lesssim \mathrm{JD} - 2\,440\,000.0 \lesssim 8977$). The astrometry could not be given with any confidence, and the transits over this period were rejected. This is unfortunately of dramatic consequence for Iapetus since only very few positions of this object were measured successfully.

4.5. Construction of the astrometric positions

The displacement on the sky of an asteroid or a planetary satellite during the ∼18 s it takes to cross the main grid, could be determined from the ephemeris with sufficient accuracy to enable the construction of a single normal position locus for each transit. For this reduction the movement of the object along the **w** direction was assumed to be linear in time and with a known velocity. A linear regression was performed over the transit in order to determine the average offset between the calculated and observed abscissae (see Fig. 11). This offset is given by a weighted mean within NDAC (L2 fit) and by the median within FAST (L1 fit); more details can be found in Hestroffer & Mignard (1997a) and Hestroffer et al. (1995). Since the normal position locus is a mean of typically eight single measurements, the corresponding error distribution will not follow a normal distribution but rather a Student's t-like distribution. The reference epochs, the standard error associated with these two estimators and the great circle on which the positions are projected are different. In contrast to the observed stars, the FAST and NDAC solutions have not been merged into a single position. The FAST reduction procedure was not adapted to the observations of the largest objects J II Europa and S VI Titan, thus only the NDAC positions are provided. For smaller objects, both procedures are valid; but, again, the FAST and NDAC positions loci do not strictly corre-

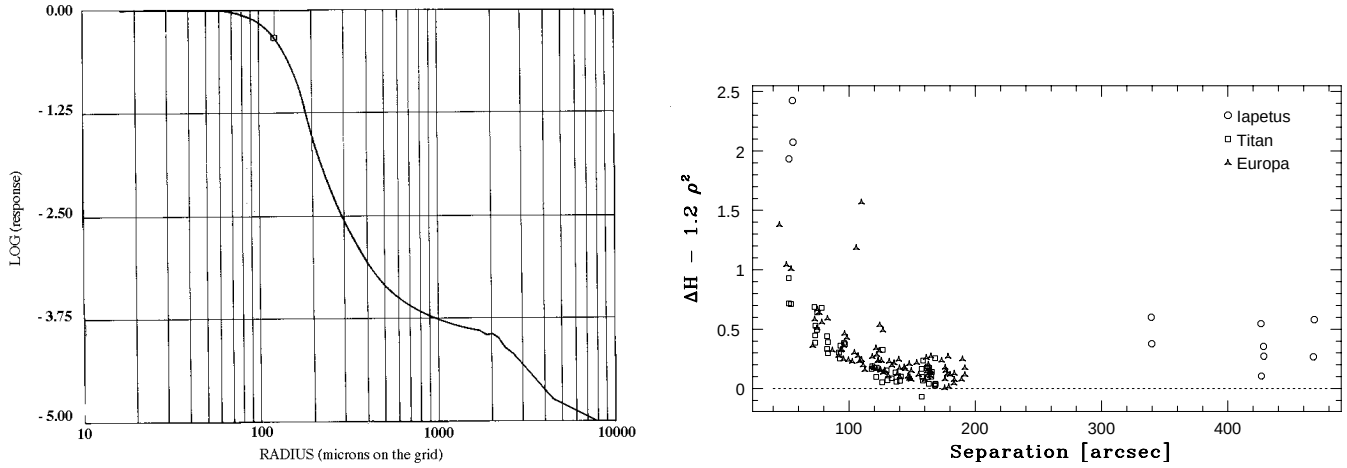

Fig. 10. Attenuation profile. Left: average profile from on-ground calibration ($8\ \mu$m$= 1.208$ arcsec). The actual in-flight profile is unknown between 100 and 500 arcsec. Right: magnitude difference ΔH corrected for bias due to the modulation as a function of the separation to the major planet

spond to the same point on the surface of the object. Hence, in order to avoid introducing additional errors, no combination of the data was performed. Nevertheless, for the smallest bodies (relative to the grid step), both FAST and NDAC loci correspond in a first approximation to the position of the photocentre (see Fig. 9).

The various steps of the reduction procedure took into account effects down to the order well below one milliarcsec. Conversely, effects not modeled with the observing precision were discarded; in particular it is stressed that no attempt has been made to account for phase, shape, or albedo corrections. The apparent directions $\mathbf{u}$ ($|\mathbf{u}| = 1$) are hence corrected for stellar aberration (due to the satellite's barycentric velocity $\mathbf{v}$, and expanded to second order in $|\mathbf{v}|/c$):

$$\mathrm{d}\mathbf{u} = -\left(1 - \frac{\mathbf{u}'\mathbf{v}}{2\,c}\right)\frac{\mathbf{v}}{c} + O\left(\frac{|\mathbf{v}|}{c}\right)^3 \tag{12}$$

yielding the 'natural' direction $\langle \mathbf{u} + \mathrm{d}\mathbf{u} \rangle$ where the notation $\langle \mathbf{x} \rangle$ denotes the unit vector $\mathbf{x}/|\mathbf{x}|$. This direction is next corrected for the general relativistic gravitational light bending due to the Sun's spherical gravitational field:

$$\mathrm{d}\mathbf{u} = -2\,\frac{m_\odot}{a}\,\tan\frac{\psi}{2}\,\langle \mathbf{u} \times (\mathbf{r}_0 \times \mathbf{u}) \rangle + O\left(\frac{m_\odot}{a}\right)^2 \tag{13}$$

where $m_\odot \sim 1.48$ km, a is the heliocentric distance of the satellite, ψ the heliocentric angle between the planet and the satellite, and $\mathbf{r}_0$ the heliocentric direction of the planet. The positions and epoch of observation are referred to the geocentre. The position locus is corrected for the Hipparcos satellite's parallax:

$$\mathrm{d}\mathbf{u} = \langle \mathbf{r}_{\rm sat} + \mathbf{u}\,\Delta \rangle - \mathbf{u} \tag{14}$$

where Δ is the distance of the planet relative to the satellite, and $\mathbf{r}_{\rm sat}$ is the known geocentric position of the Hipparcos satellite.

Some transits were discarded during one or other of the consortia's great circle data reductions, and also during the transit reductions. The latter correspond essentially to measurements corrupted by parasitic light (for example due to the parent planet in the case of planetary satellites, or veiling glare by a star) and/or in the case of a badly centred instantaneous field of view. Dubious abscissae v with rms greater than 150 mas were systematically discarded. Observations of planetary satellites taking place with a separation to the planet less than 70 arcsec were also systematically rejected. In order to identify transits possibly corrupted by the presence of a parasitic object in the complementary field of view, FAST observations with $\sigma_{\Delta H} = \sigma_{(H_{p_{\rm ac}} - H_{p_{\rm dc}})} > 0.3$ were rejected. Similarly transits of satellites occurring when another bright satellite was in the field of view at distances of less than 26 arcsec were also rejected.

Two others tests were constructed to filter out unreliable data. Transits for which the observed movement was inconsistent with the predicted one, i.e. with an estimated mean error per unit weight of the residuals $\tilde{\sigma}_0$ such that $\tilde{\sigma}_0 > 2\,\sigma_0$, were rejected. Also, transits containing only one frame, instead of the typically eight frames, were systematically rejected. Likewise, a grid-crossing of a minor planet yielding a magnitude difference between the ac– and dc–scales such that:

$$|\Delta H - \Delta H_{\rm calc}| > 5\,\sigma_{\Delta H} \tag{15}$$

was removed. Here $\Delta H_{\rm calc} \sim 1.214\,\rho^2 + 0.03\,\rho^4$ is derived from Eqs. (8) and (11) for an object of uniform brightness and of apparent diameter ρ. Transits rejected during the astrometric reduction were also discarded for the photometric output.

The epoch of observation was also corrected for the first order light-time difference due to the geocentric orbit. Hence the published position corresponds to the astrometric direction at time $t - \tau$, where t is the published epoch of observation and τ is the light-time delay to the geocentre. The epoch at the Hipparcos satellite can be calculated by $t' = t - \Delta\tau$ where the difference $\Delta\tau \equiv \tau' - \tau$ is provided as additional data. Since the latter is a small quantity when compared to the time resolution of the basic measurement, no use of a special relativistic formalism has been made; this time offset is then calculated as:

$$\Delta\tau \equiv \tau' - \tau = \frac{EP - SP}{c} \tag{16}$$

where EP and SP are respectively the geocentric and satellitocentric distances of the planet apparent position, and c the velocity of light.

The astrometric direction for each transit is supplied by means of a reference point $(\alpha_0,\, \delta_0)$ and the direction of the straight line $v =$ constant in the tangent plane associated with this reference point (see Fig. 7). The reference point is constructed in such a way that it has the same observed abscissa on the reference great circle ($v = v^{\rm obs}$), and an ordinate given by the calculated ephemeris ($r = r^{\rm calc}$). The direction of the observed position locus is given in the tangent plane by the position angle θ reckoned positive from north through east. The standard error in the **w** direction is given by $\sigma_{v*} = \sigma_v\, \cos r^{\rm calc}$. There is no astrometric measurement, and thus no similar quantity, along the perpendicular direction $(\theta \pm \pi/2)$. All positions are referred to the ICRS(Hipparcos) system (see Sect. 5).

When comparing the published coordinates with independent two-dimensional equatorial coordinates $(\alpha^c,\, \delta^c)$ - which may be either calculated or observed - the strictly one-dimensional nature of the Hipparcos observations must be taken into account, since the published direction $(\alpha_0,\, \delta_0)$ effectively constrains the position in only this single dimension. Thus, for comparison with the observed positions, the residuals (i.e. the differential equatorial coordinates):

$$\begin{pmatrix} \Delta\alpha* \\ \Delta\delta \end{pmatrix} = \begin{pmatrix} (\alpha_0 - \alpha^c)\, \cos\delta_0 \\ \delta_0 - \delta^c \end{pmatrix} \tag{17}$$

should be projected onto the great circle, from which only the single equation of condition is retained:

$$\Delta v = v^{\rm obs} - v^c \sim (\, \sin\theta \quad \cos\theta\,) \cdot \begin{pmatrix} \Delta\alpha* \\ \Delta\delta \end{pmatrix} \tag{18}$$

where small terms due to the projection from the celestial sphere to the tangent plane are neglected. Similarly, the photocentre offset in the direction of the Sun, when $\theta_{\rm s}$ is the position angle of the sub-solar point, is under the condition of a symmetric brightness distribution with respect to the intensity equator (Lindegren 1987):

$$\delta v_{\rm phot} = \cos(\theta - \theta_{\rm s})\; C(i)\; \sin(i/2)\; \rho/2 \tag{19}$$

where i is the solar phase angle, and $C(i)$ is a function depending on the scattering properties of the object's surface.

5. Transformation to the ICRS

5.1. The optical ICRS(Hipparcos)

After the sphere reduction stage, the astrometric positions of all Hipparcos or Tycho solar system objects are linked to intermediate reference frames P (called F37.3 for FAST, N37.5 for NDAC and for historical reasons N18 for TDAC). However the positions have to be given in the system of the final Hipparcos Catalogue, i.e. the optical counterpart of the ICRS. The astrometric Hipparcos Catalogue is not a fundamental catalogue in the sense that the positions and proper motions of stars were determined to a time-variable rotation. Thus the frame P associated with each sphere solution, although homogeneous, is arbitrary. All the reference frames P are defined by the stars and the associated sphere construction; they are related to the single sphere solution H37C (Lindegren et al. 1997). This latter reference frame was next aligned to the frame of the ICRS by a small time-dependent rotation $\boldsymbol{R}(\boldsymbol{\varepsilon})$ along the axis of positive rotation $\langle\boldsymbol{\varepsilon}\rangle$ (Lindegren & Kovalevsky 1995; Kovalevsky 1997):

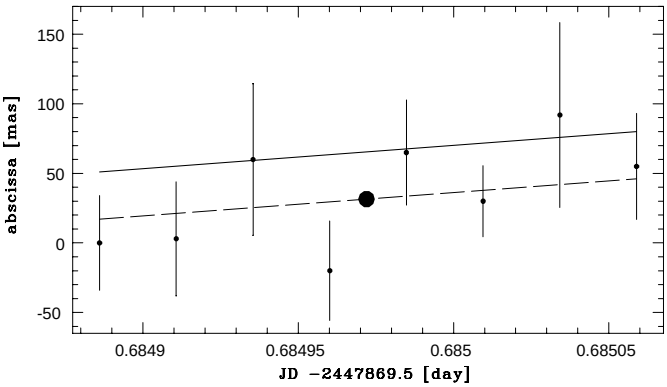

Fig. 11. Reduction of a minor planet abscissae v at the transit level. A normal place for each transit is constructed by fitting the location parameter of a linear motion whose speed is taken from the ephemeris (solid line). The normal position (filled circle) corresponds to an average position of the frame level positions (mean in NDAC, median in FAST). The plot is drawn for a FAST transit; the great circle abscissa origin is arbitrary

$$\boldsymbol{\varepsilon}(t) = \boldsymbol{\varepsilon}_0 + (t - T_0)\, \boldsymbol{\omega} \tag{20}$$

where T_0 is the reference epoch ($T_0 =$ J1991.25). The orientation and spin components of these intermediate frames with respect to the ICRS are given with a precision estimated to be 0.6 mas for the orientation and 0.25 mas/year for the spin components (Kovalevsky et al. 1997).

5.2. Transformation of equatorial coordinates

Since the system P is tied to the system of the ICRS by an infinitesimal rotation, the transformation of the astrometric direction $\mathbf{u}_{\rm P}(t)$ of either the Hipparcos reference point $(\alpha_0,\, \delta_0)_{\rm P}$ or the Tycho equatorial coordinates $(\alpha,\, \delta)_{\rm P}$ is given by:

$$\mathbf{u}_{\rm ICRS}(t) = \begin{pmatrix} 1 & \varepsilon_z & -\varepsilon_y \\ -\varepsilon_z & 1 & \varepsilon_x \\ \varepsilon_y & -\varepsilon_x & 1 \end{pmatrix} \mathbf{u}_{\rm P}(t) \tag{21}$$

where $\varepsilon_x, \varepsilon_y, \varepsilon_z$, the equatorial components of $\boldsymbol{\varepsilon}(t)$ for the epoch of observation, are of the order of a few tens of milli-arcsec. In principle, the transformation for the Hipparcos position locus entails also a change of the position angle θ, but this change would always be less than 0.1 arcsec and was therefore neglected. For the Tycho data the spin components between the two reference frames are of the order of 1 mas/year and are negligible. Zonal and temporal systematic errors of larger size (up to 6 mas) were also neglected with regard to the random error

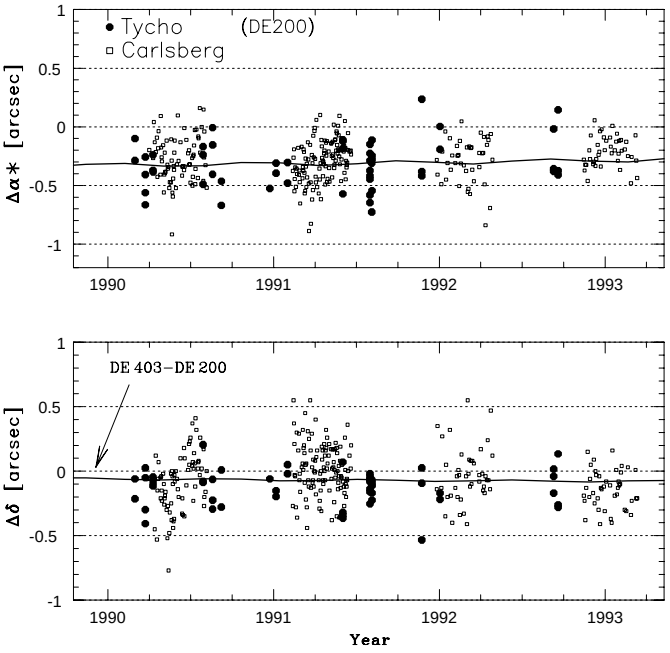

Fig. 12. Residuals for the Tycho and Carlsberg positions of Uranus relative to the DE200 ephemeris. Each point corresponds to a single transit across each instrument. The solid line corresponds to the DE403 ephemeris

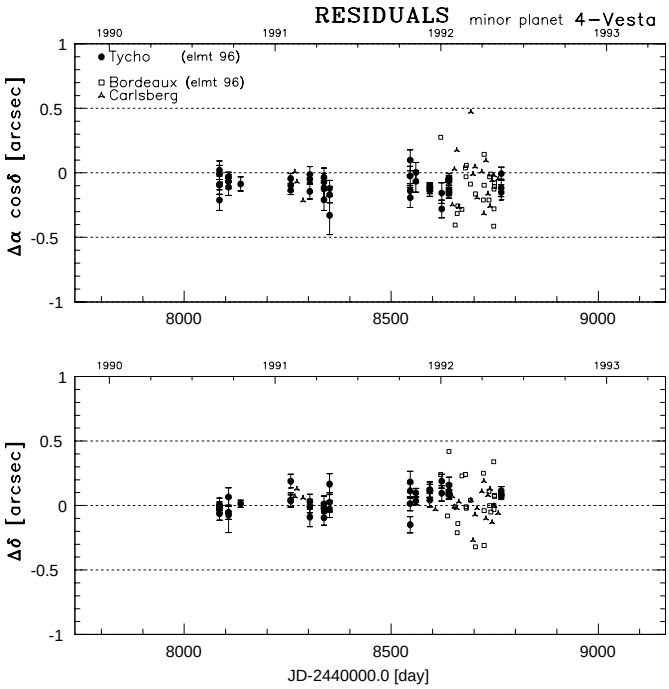

Fig. 13. Residuals for the Tycho, Carlsberg and Bordeaux positions of minor planet (4) Vesta. The russian osculating elements for the year 1996 were taken for the calculation of the ephemeris. Each point corresponds to a single transit across each instrument

of a Tycho single transit. For the Hipparcos data, the transformation of the astrometric direction could also be applied on the coordinates of the reference great circle and the the abscissa v. The formulation derived by Söderhjelm & Lindegren (1982) and given by their Eqs. (17) and (18) is equivalent to the one given here.

6. Comparisons and precisions

The Tycho positions have some similarities with the coordinates obtained by meridian circle observations. The number of transits per apparition may however be considerably smaller, and since these occur around the quadratures, they are complementary to the ground-based measurements. Fig. 12 shows the Tycho residuals obtained for Uranus with respect to the widely used DE200 ephemeris. These are given together with the residuals obtained with the Carlsberg instrument at La Palma. Both observational data are in good agreement; in particular they show the systematic error in right ascension of the DE200 solution and the improvement obtained with the DE403 solution. It was noted in Sect. 3 that the formal precision of the Tycho observations are mostly indicators of the quality of the astrometric measurements. As can be seen from the dispersion of the residuals, the Tycho positions are of the same order of precision as the ground-based observations carried out with meridian circles. Fig. 13 shows the residuals for the minor planet (4) Vesta together with those obtained with the Carlsberg instrument and the meridian circle at Bordeaux. For this minor planet the Tycho data provide a valuable complement to the best ground-based astrometric observations.

The FAST and NDAC one-dimensional astrometric results from Hipparcos have been obtained by independent means. They differ mainly by the fact that they have not been derived for the precisely same epoch, neither do they correspond to projections on the same great circle, and they do not correspond to the same point on the surface of the asteroid (see Sect. 4). If we consider the subset of the 39 asteroids of size smaller than 0.2 arcsec[1], the correlation factor of 0.85 between the abscissae and the scaling of the standard errors as derived from faint stars (Arenou, private communication), we find the distribution of the normalised difference $\Delta v/\sigma_v$ given in Fig. 14. As expected, this distribution is an almost centered Gaussian of unit variance (with a mean $\langle \Delta v \rangle < 1$ mas), so that no significant systematic offset is present between the FAST and NDAC positions for this subset of observations.

The precision of the Hipparcos photometric and astrometric data of the transit level depend on the magnitude of the object at the observation epoch. The standard errors for the Hipparcos astrometry are given in Fig. 15. With an average of $10-15$ mas, the Hipparcos measurements, which are directly related to the ICRS, surpass in quality the ground-based meridian telescopes observations by a factor $\sim$10. Fig. 16 shows the distribution of the standard errors for the more precise dc photometric component. The average precision of the transit level is $0.02-0.03$ mag. Since the dc– and ac–components are independent, a more precise estimator can be constructed by taking

[1] Excluding the nine asteroids (1) Ceres to (7) Iris, (10) Hygiea and (324) Bamberga

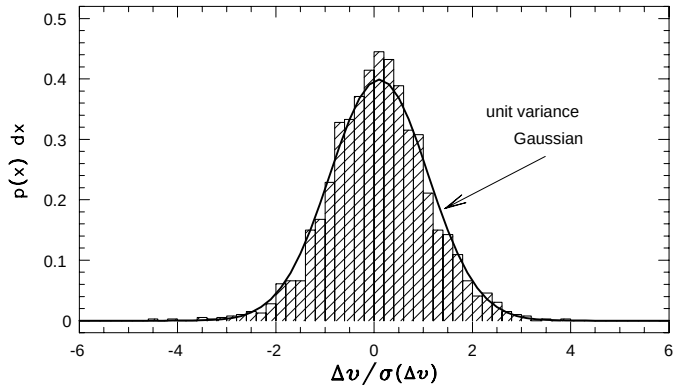

Fig. 14. Normalised difference between the FAST and NDAC positions. The histogram is constructed from a subset of 39 minor planets and a total of 1967 transits in common between the NDAC and FAST catalogues

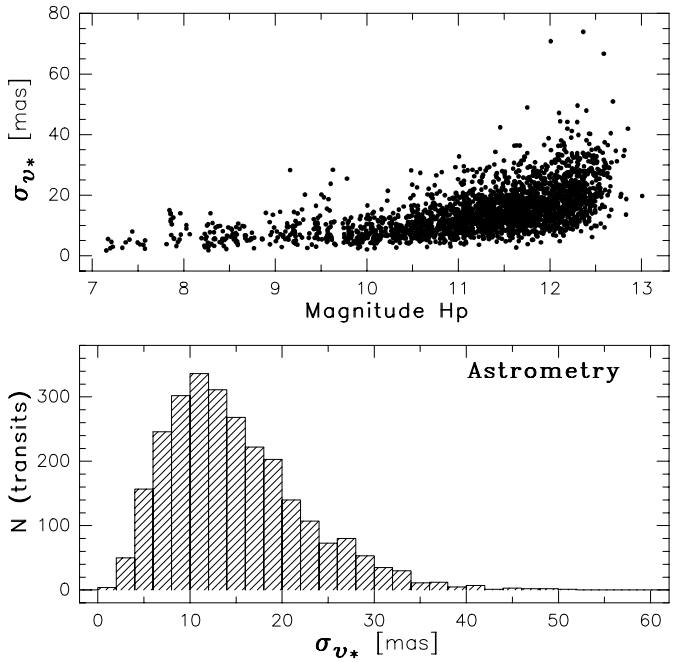

Fig. 15. Standard errors for the Hipparcos astrometry σ_{v*} as a function of apparent magnitude (top) and histogram (bottom) for a total of 2665 FAST transits

the (weighted) mean of the $Hp_{\rm ac}$ and $Hp_{\rm dc}$ values; however such a construction introduces systematic errors when the object's angular size is not negligible (i.e. when the modulation coefficients are such that $M > M_o$ and/or $N > N_o$, see Sect. 4).

7. Conclusions and future prospects

The Hipparcos satellite has provided valuable astrometric and photometric data for a total of 55 relatively bright solar system objects (mainly asteroids, but also planetary satellites and major planets). The observations are spread over the period ranging from end of November 1989 to the middle of March 1993. The Tycho measurements are of lower precision than the - main mission - Hipparcos ones, but are extended to larger objects. Tycho

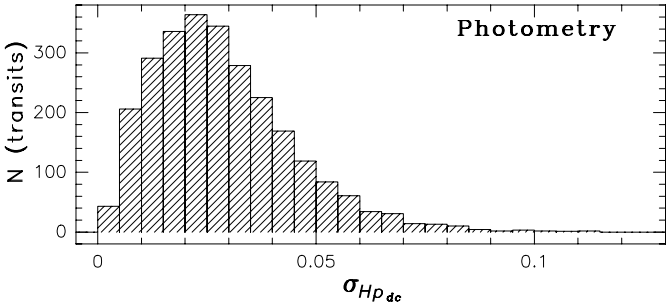

Fig. 16. Standard errors for the Hipparcos photometry. The histogram corresponds to the $Hp_{\rm dc}$ magnitude for a total of 2639 transits

provides conventional astrometric positions in right ascension and declination, and photometry in two filters close to the Johnson B and V bands. Hipparcos provides one-dimensional astrometric positions, and photometry in the broad-band Hp photometric system. All astrometric positions are referred to the ICRS, and epochs are given in the TT time scale.

The results are gathered in the Hipparcos and Tycho Catalogues of solar system objects appearing in Volume 10 (printed format) of The Hipparcos and Tycho Catalogues (ESA 1997), and in the ASCII CD-ROMs (Volume 17). They are also accessible via the Centre de Données astronomique[2] at Strasbourg (France). Descriptions of the catalogue contents can be found in these different documents.

As far as solar system objects are concerned, Hipparcos yields not only valuable information by direct observations of these objects, but also by the very accurate astrometric positions of reference stars in photographic plates or CCD (re-)reductions. Hipparcos also provide a strong basis for future astrometric missions. GAIA (Global Astrometric Interferometer for Astrophysics) proposed by Lindegren & Perryman (1996) within the the context of ESA's 'Horizon 2000 Plus' programme would allow astrometric observations at the submilliarcsecond level for several hundreds of small asteroids (Hestroffer & Morando 1995). It would also provide high precision photometry in a way similar to Hipparcos. In contrast to Hipparcos, GAIA would be able to resolve hundreds of asteroids (and also stars), leading for the first time to the determination of their diameters in the optical domain, and also to a basis of comparison with the extensive results obtained from the IRF method by the IRAS satellite.

Acknowledgements. The authors are grateful to the many people involved in the INCA, FAST, NDAC and TDAC Consortia without whom this work would not have been possible. We would like to acknowledge in particular U. Bastian, J.-L. Falin, M. Froeschlé, V.V. Makarov, C.A. Murray and M.A.C. Perryman for their dedicated contribution.

Special thanks are also addressed to J.-E. Arlot, A. Bec-Borsenberger, J. Berthier and W. Thuillot for their assistance in the ephemerides calculation, and to M. Rapaport and L.V. Morisson for providing us with the ground-based observations of La Palma and Bordeaux.

[2] http://cdsweb.u-strasbg.fr
ftp://cdsarc.u-strasbg.fr/cats/I/239

D. Hestroffer is supported by a research grant from the European Space Agency.

References

Arlot J.E., 1982, A&A 107, 305
Batrakov Y.V., 1991, Ephemerides of minor planets for the year 1992, Institute of Theoretical Astronomy, St Petersburg
Bastian U., Wagner K., 1997, In: The Hipparcos and Tycho Catalogues. ESA SP–1200 Vol. 4, 91
Bec-Borsenberger A., 1985, In: Scientific aspects of the Input Catalogue. ESA SP–234, 175
Bec-Borsenberger A., 1989, In: The Hipparcos mission Vol. 2. ESA SP–1111, 213
Bec-Borsenberger A., Bange J.-F., Bougeard M.-L., 1995, A&A 304, 176
Bowell E., Hapke B., Domingue D., et al., 1989, In: Asteroids II, R.P. Binzel, T. Gehrels, M.S. Shapley (eds), The University of Arizona Press, p. 524
Bretagnon P., 1982, A&A 114, 278
Chapront-Touzé M., Chapront J., 1983, A&A 124, 50
Clemence G.M., 1948, AJ 54, 10
Dourneau G., 1993, A&A 267, 292
Dyson F., 1928, Trans. IAU 3, 227
ESA, 1997, The Hipparcos and Tycho Catalogues. ESA SP–1200
Fienga A., Arlot J.-E., Pascu D., 1997, In: The Hipparcos Venice97 Symposium. ESA SP–402, 157
Folkner W.M., Charlot P., Finger M.H., et al., 1994, A&A 287, 279
Fricke W., 1982, A&A 107, L13
Großmann V., 1997, In: The Hipparcos and Tycho Catalogues. ESA SP–1200 Vol. 4, 123
Harris A.W., Lupishko D.F., 1989, In: Asteroids II, R.P. Binzel, T. Gehrels, M.S. Shapley (eds), The University of Arizona Press, p. 39
Hestroffer D., Mignard F., 1997a, In: The Hipparcos and Tycho Catalogues. ESA–SP 1200 Vol. 3, 305
Hestroffer D., Mignard F., 1997b, A&A 325, 1253
Hestroffer D., Morando B., 1995, In: Future possibilities for astrometry in space. Joint RGO-ESA workshop, Cambridge, UK, 19-21 june 1995. ESA SP-379, 41
Hestroffer D., Morando B., Mignard F., Bec-Borsenberger A., 1995, A&A 304, 168
Hilton J.L., 1997, AJ 114, 402
Høg E., Hestroffer D., Makarov V.V., 1997, In: The Hipparcos and Tycho Catalogues. ESA SP–1200 Vol. 4, 205
Kovalevsky J., 1997, In: The Hipparcos Venice97 Symposium. ESA SP–402, 11
Kovalevsky J., Lindegren L., Perryman M.A.C., et al., 1997, A&A 323, 620
Lindegren L., 1987, In: Third FAST thinkshop, 3-6 Nov. 1986, Bari (Italy). P.L. Bernacca and J. Kovalevsky (eds.), p. 285
Lindegren L., Kovalevsky J., 1995, A&A 304, 189
Lindegren L., Perryman M.A.C., 1996, A&AS 116, 579
Lindegren L., Frœschlé M., Mignard F., 1997, In: The Hipparcos and Tycho Catalogues. ESA SP–1200 Vol. 3, 323
Mignard F., Evans D., van Leeuwen F., 1997, In: The Hipparcos and Tycho Catalogues. ESA SP–1200 Vol. 3, 273
Morando B., 1987, In: Third FAST thinkshop, 3-6 Nov. 1986, Bari (Italy). P.L. Bernacca and J. Kovalevsky (eds.), p. 277
Morando B., Lindegren L., 1989, In: The Hipparcos mission. ESA SP–1111 Vol. 3, 269
Morrison L.V., Hestroffer D., Taylor D.B., van Leeuwen F., 1997, In: The Hipparcos Venice97 Symposium. ESA SP–402, 149
Scholl H., Schmadel L.D., Röser S., 1987, A&A 179, 311
Söderhjelm S., Lindegren L., 1982, A&A 110, 156
Standish E.M. Jr., 1990, A&A 233, 352
van Leeuwen, Evans D.W., Grenon M., et al., 1997, A&A 323, L61
Viateau B., Rapaport M., 1997, A&A 320, 652